

Supporting Information

Photoresponsive proton conduction in Zr-based metal-organic frameworks using the photothermal effect

Ming-Feng Qin, Chang-Yu Wang, Song-Song Bao,* and Li-Min Zheng*

Experimental section

Materials and instrumentation. The [5, 10, 15, 20-tetrakis (*p*-phenylphosphonic acid) porphyrin-nickel(II)] (Ni-TPPP) and [5, 10, 15, 20-tetrakis (*p*-phenylphosphonic acid) porphyrin] (H₁₀TPPP) were synthesized according to the reported method.¹⁻³ All the other chemicals purchased from a commercial resource except organic ligands were used as received without additional purification. The infrared (IR) spectroscopy in the range of 400-4000 cm⁻¹ was taken on a Bruker Tensor 27 spectrometer at room temperature. Elemental analyses for C, H, and N were performed on an Elementar Vario Macro cube. Powder X-ray diffraction (PXRD) data were collected on a Bruker Advance D8 diffractometer with Cu-K_α radiation ($\lambda = 1.5406 \text{ \AA}$) at room temperature in a range of 3-50°. Thermogravimetric analysis was collected on a Mettler-Toledo TGA/DSC 1 instrument in the range of 30-600 °C with a heating rate of 5 °C min⁻¹ under a nitrogen flow (20 mL·min⁻¹). UV-Vis-NIR spectra of solid-state powder samples were measured on a Shimadzu UV-3600 spectrophotometer with barium sulfate powder as a reference with the wavelength range 400-1600 nm⁻¹ at room temperature. The UV-Vis-NIR spectra for sample dispersion was collected on a Shimadzu UV-3600 spectrophotometer with deionized water as a reference. Adsorption/desorption isotherms were measured using a BELSORP max instrument (BEL Japan, Inc.). Scanning electron microscope (SEM) was carried out on JEOL JSM-7800F. The Fotric 226s IR camera collected infrared photographs. An 808 nm light was generated through an infrared diode laser generator (MW-GX-808/5W from Changchun LASER Optoelectronics Tech Co, Ltd.), and the spot area is 1 cm². A white light was generated by a Xe-lamp (CEL-PF300-T9) with a power density of 0.1-0.5 W cm⁻² measured by a CEL-NP2000-2 optical Power meter.

Specific heat capacity measurement and calculation. The specific heat capacity (C_p) is obtained by the instrument of Flash DSC 1 (Mettler Toledo, Switzerland) with an intracooler (TC100MT, Huber). The DSC was performed at a heating rate of 10 K/min under an inert atmosphere of nitrogen gas at a flow rate of 50 mL/min between the temperature range of 30 to 120 °C. A two-cycle scan was performed included baseline correction and standard reference material (sapphire) and the tested sample powder. The mass of sapphire, **1** and **2** are 21.8, 4.2 and 5.1 mg, respectively. The C_p value of **1** and **2** are

calculated by the following Equation (1)⁴:

$$C_p = \frac{DSC_{sample} - DSC_{baseline}}{DSC_{sapphire} - DSC_{baseline}} \cdot C_{p,sapphire} \quad (1)$$

in which C_p is the specific heat of the sample at specified temperature. $C_{p, sapphire}$ is the specific heat of sapphire. $(DSC_{sample} - DSC_{baseline})$ and $(DSC_{sapphire} - DSC_{baseline})$ are the recorded DSC signal of the sample or sapphire with baseline correction. The average C_p values of compound **1** and **2** in the temperature range 30 – 100 °C are 0.94 and 1.11 J/g·°C, respectively.

Photothermal conversion efficiency calculation. The photothermal conversion efficiency (η) is an essential parameter in practical application and is conventionally defined as the ratio of the internal energy increase of the material to the total incident light radiation. For solid samples, the η value is calculated by the following Equation (2)⁵:

$$\eta = \frac{c_p m \Delta T}{I A \Delta t} \quad (2)$$

where C_p , m , and ΔT represent the solid sample's specific heat capacity, mass, and temperature change. I , A , and Δt represent the light intensity, irradiated area, and irradiation time. Thermal energy absorbed by the air is negligible. The values of these parameters for **1** are $C_{p,1}$ (0.94 J/g·°C), m_1 (14.3 mg), ΔT (65.8 °C), I (0.5 W/cm²), A (0.14 cm²) and Δt (180 s). The the values of these parameters for **2** are $C_{p,2}$ (1.11 J/g·°C), m_1 (14.8 mg), ΔT (58.5 °C), I (0.5 W/cm²), A (0.145 cm²) and Δt (180 s). Consequently, the determined η values of compounds **1** and **2** irradiated by 808 nm laser with a power density of 0.5 W/cm² are 7.1% and 7.4%, respectively.

Proton conductivity measurements. Two rectangular pellets of **1** (5.0×2.8×0.721 mm³) and **2** (5.0×2.9×0.742 mm³) were prepared under a pressure of 0.075 GPa to study their humidity-dependent and temperature-dependent conductivities. Another rectangular pellets of **1** (5.0×3.0×0.650 mm³) and **2** (5.0×2.8×0.746 mm³) were prepared to examine the influence of the photothermal effect on the proton conductivity. **1@PMMA** and **2@PMMA** was prepared by soaking the pellets of **1** and **2** in an acetone solution of PMMA and drying it in the air. The conductivities of sample pellets were obtained by AC impedance

measurements, which were carried out under controlled environmental conditions using the conventional quasi-four-probe method with a Solartron SI 1260 Impedance/Gain-Phase Analyzer 1296 Dielectric Interface in the frequency range 1.0 MHz – 0.1 Hz. The electrical contacts were connected using silver paste (SPI-PAINT) to attach the 50 μm diameter gold wires to both lateral sides of the pellets. The environmental conditions (55-95% RH and 15-55 $^{\circ}\text{C}$) were controlled using a GSJ-100A (Su-Ying Corp.) humidity-controlled oven. A closed glass box containing water was used to expose the sample pellet in the saturation water vapour ($\sim 100\%$ RH).

The proton conductivity values σ and active energy E_a were estimated using the following Equation:

$$\sigma = \frac{l}{RA} \quad (3)$$

$$\ln(\sigma T) = \ln\sigma_0 - \frac{E_a}{k_B T} \quad (4)$$

where l , R , A , T , and σ_0 represent two-electrode distance, the electrode's area, the sample's resistance, temperature, and a pre-exponential factor. R values were obtained by fitting the first semi-circle in the high-frequency range of Nyquist plots or estimated to X-intercept of the low-frequency tail without an obvious high-frequency semi-circle due to the bulk impedance. E_a values were obtained from Arrhenius plots of $\ln(\sigma T)$ vs. $1000/T$.

Synthesis of $[\text{Zr}_2(\text{H}_4\text{TPPP})(\text{OH}/\text{F})_2] \cdot x\text{H}_2\text{O} \cdot \text{ZrO}_2$ (1**).** The synthetic procedure is similar to the literature reported.³ H_{10}TPPP (29.7 mg, 0.032 mmol), $\text{ZrOCl}_2 \cdot 8\text{H}_2\text{O}$ (19.6 mg, 0.066 mmol) and NaF (76.4 mg, 1.9 mmol) were added into deionized water (6 mL) and sonicated for 10 min. Subsequently, the brick-red suspension was adjusted to pH = 8.0 by sodium hydroxide solution (2 M). The reactants were transferred into a 20 mL Teflon-sealed autoclave and heated at 160 $^{\circ}\text{C}$ for 24 h. After cooling down to room temperature, the reddish-brown powder of **1** was separated by centrifugal at 16000 rpm for 10 min and washed twice with deionized water and acetone. The obtained sample was dried at room temperature, affording a yield of 64.6% (based on H_{10}TPPP). Anal. calcd for $\text{C}_{44}\text{H}_{28}\text{N}_4\text{O}_{14}\text{P}_4\text{F}_2\text{Zr}_3 \cdot 34\text{H}_2\text{O}$ (Mw 1884.78): C, 28.04; H, 5.13; N, 2.97 (%). Found: C, 27.55; H, 4.89; N, 2.75%. IR (KBr pellet): 3439(m), 1634(m), 1557(vw), 1497(vw), 1473(vw), 1396(w), 1352(vw), 1139(m), 1029(s), 1005(s), 981(s), 855(w), 804(m), 737(m), 587(s),

451(w) cm^{-1} .

Synthesis of $[\text{Zr}_2(\text{Ni-H}_2\text{TPPP})(\text{OH/F})_2]\cdot x\text{H}_2\text{O}\cdot\text{ZrO}_2$ (2). The synthesis procedure was similar to **1**, except the H_{10}TPPP ligand was replaced with $\text{Ni-H}_8\text{TPPP}$ (30.0 mg, 0.032 mmol). Yield: 82.8% (based on $\text{Ni-H}_8\text{TPPP}$). Anal. calcd for $\text{C}_{44}\text{H}_{26}\text{N}_4\text{O}_{14}\text{P}_4\text{F}_2\text{Zr}_3\text{Ni}\cdot 30\text{H}_2\text{O}$ (Mw 1869.41): C, 28.27; H, 4.64; N, 3.00 (%). Found: C, 27.94; H, 4.42; N, 2.63%. IR (KBr pellet): 3437(m), 1631(m), 1551(vw), 1491(vw), 1461(vw), 1393(s), 1352(vw), 1137(m), 1020(m), 985(s), 855(w), 799(m), 738(m), 716(m), 595(s), 504(m), 488(w) cm^{-1} .

References

1. T. Yamamura, S. Suzuki, T. Taguchi, A. Onoda, T. Kamachi and I. Okura, *J. Am. Chem. Soc.*, 2009, **131**, 11719-11726.
2. T. Rhauderwiek, K. Wolkerdörfer, S. Øien-Ødegaard, K.-P. Lillerud, M. Wark and N. Stock, *Chem. Commun.*, 2018, **54**, 389-392.
3. T. Rhauderwiek, H. Zhao, P. Hirschle, M. Döblinger, B. Bueken, H. Reinsch, D. D. Vos, S. Wuttke, U. Kolb and N. Stock, *Chem. Sci.*, 2018, **9**, 5467-5478.
4. B. Wu and K. S. Walton, *J. Phys. Chem. C.*, 2011, **115**, 22748-22754.
5. D. Yang, B. Zhou, G. Han, Y. Feng, J. Ma, J. Han, C. Liu and C. Shen, *ACS Appl. Mater. Interfaces*, 2021, **13**, 8909-8918.

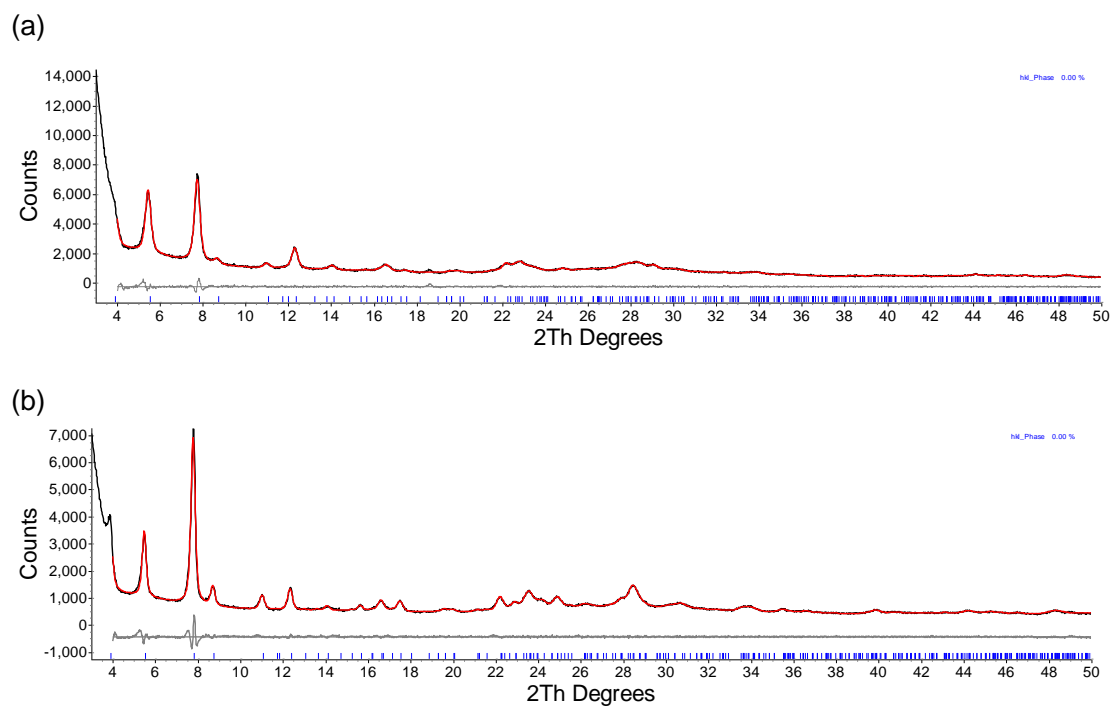


Figure S1. The pawley refinements of **1** (a) and **2** (b). The result for **1**: $I4_1/acd$, $a = 45.207 \text{ \AA}$, $c = 8.051 \text{ \AA}$, $V = 16453.1 \text{ \AA}^3$, $R_{wp} = 4.09$; for **2**: $I4_1/acd$, $a = 45.218 \text{ \AA}$, $c = 7.920 \text{ \AA}$, $V = 16194.6 \text{ \AA}^3$, $R_{wp} = 3.98$.

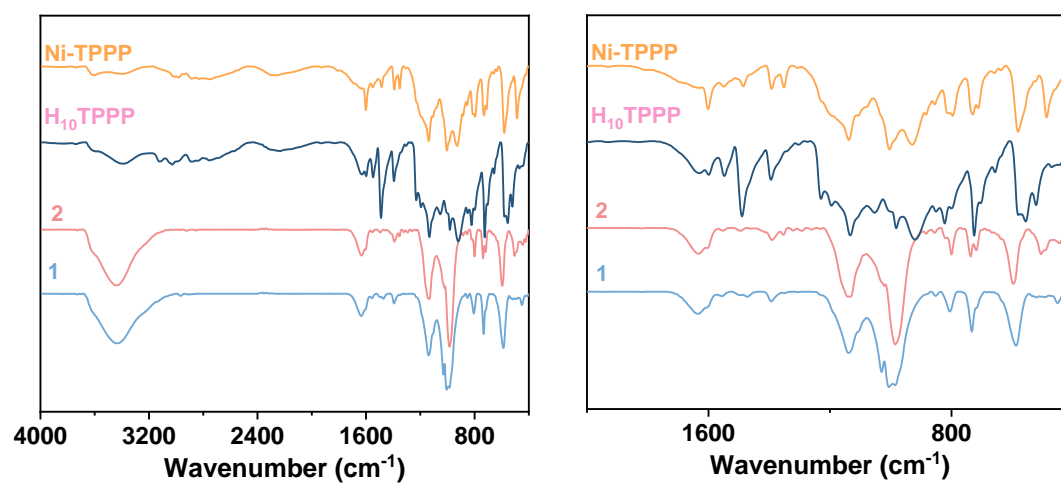


Figure S2. IR spectra of $H_{10}TPPP$, $Ni^{II}-H_8TPPP$, **1** and **2**.

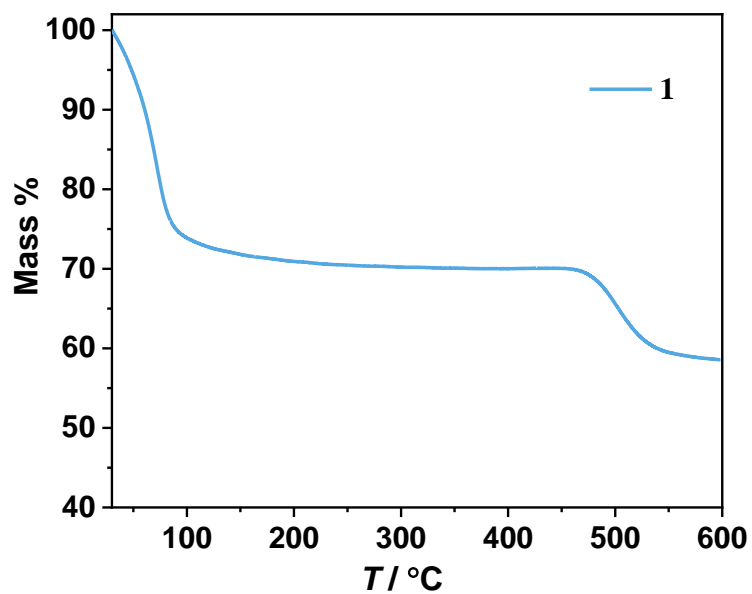


Figure S3. The TGA curve of **1**.

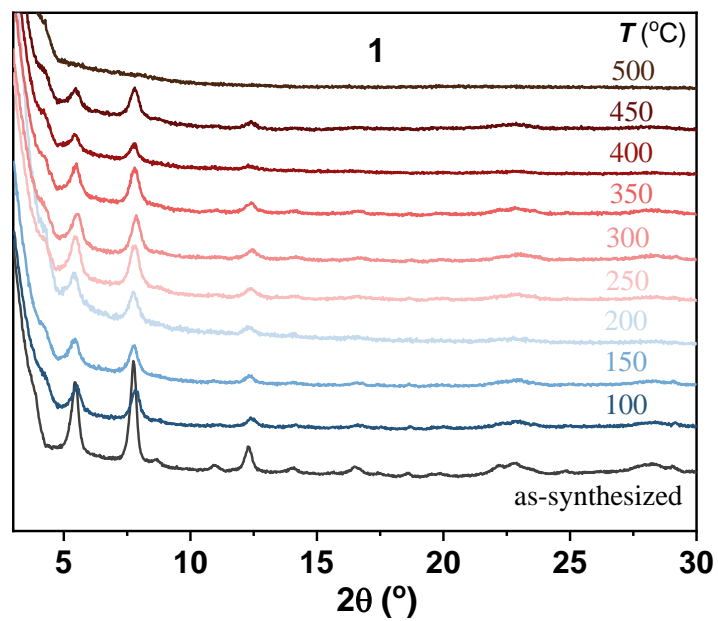


Figure S4. The variable temperature PXRD patterns of **1** upon heating from room temperature to 500 °C under vacuum.

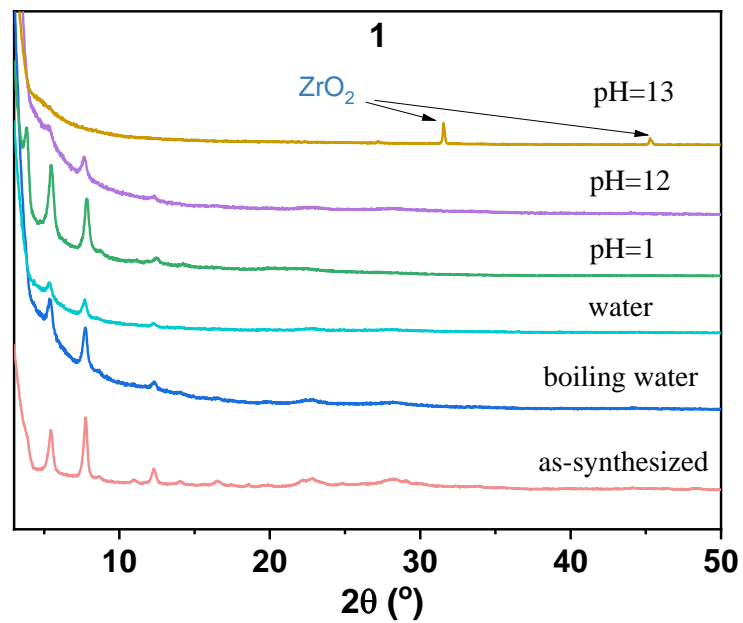


Figure S5. The PXRD patterns of the as-synthesized and post-treated samples of **1** by soaking in boiling water and different HCl/NaOH aqueous solutions in the pH range of 1 to 13.

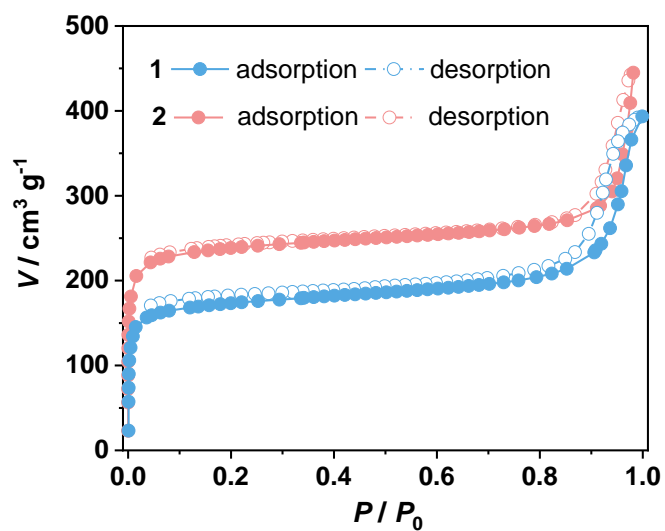


Figure S6. The N_2 sorption isotherms at 77 K of **1** and **2**.

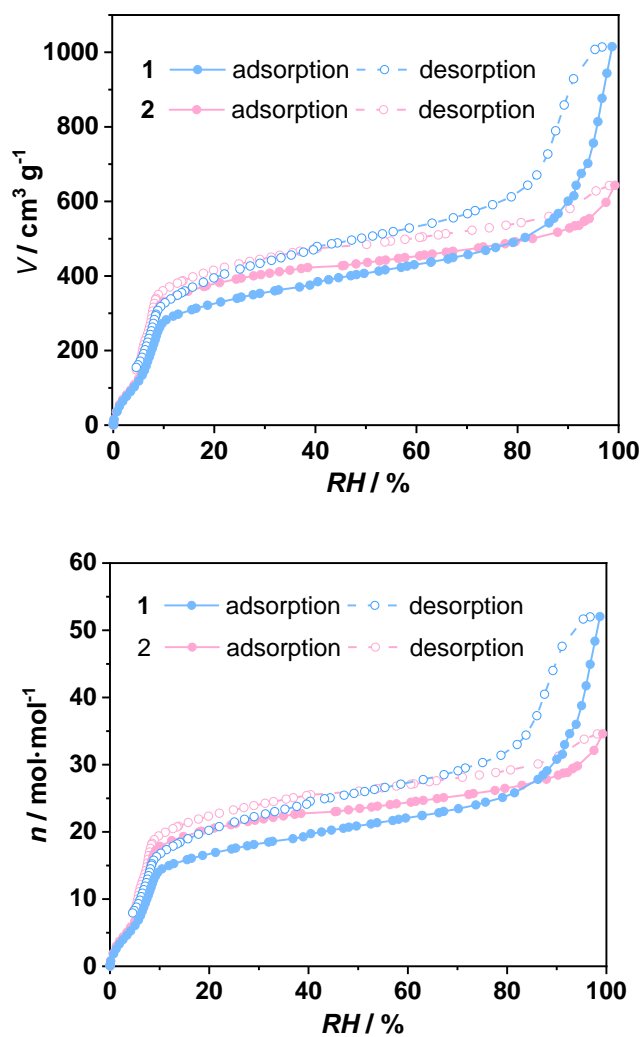


Figure S7. Water sorption isotherms at 298 K of **1** and **2** (Top and down graphs show different Y-coordinates).

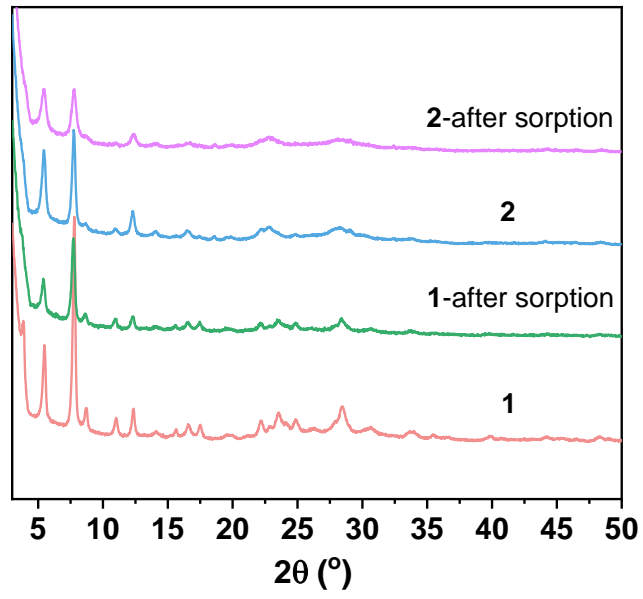


Figure S8. The PXRD patterns of **1** and **2** before and after the water adsorption/desorption process.

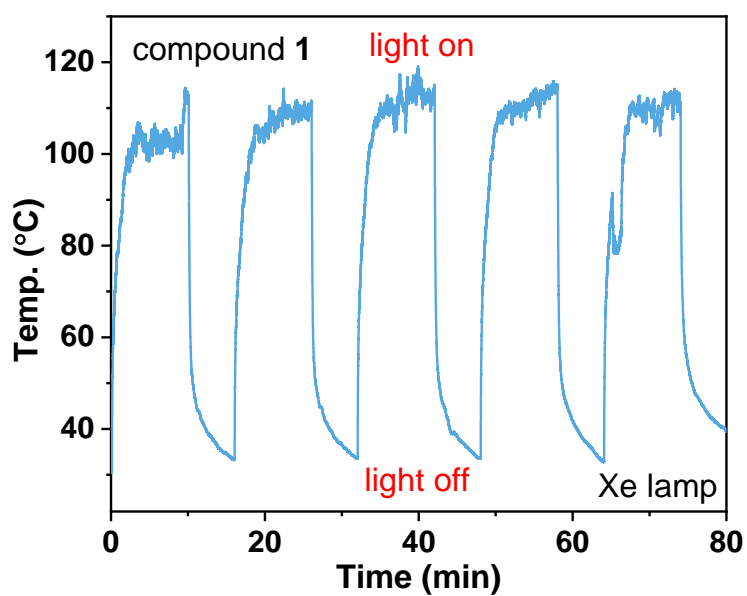
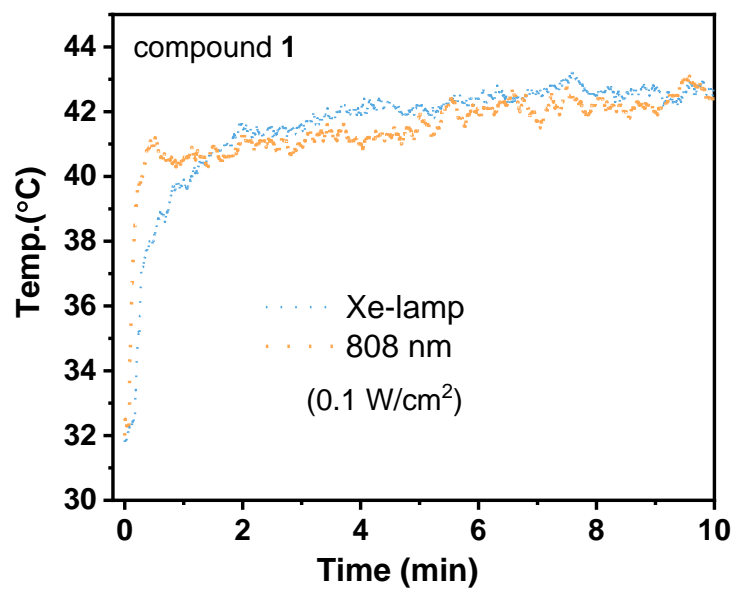


Figure S9. Plots of temperature versus time of **1** under Xe-lamp irradiation with a power density of 0.1 W/cm² and five cycles of light on/off under Xe-lamp irradiation with a power density of 0.5 W/cm².

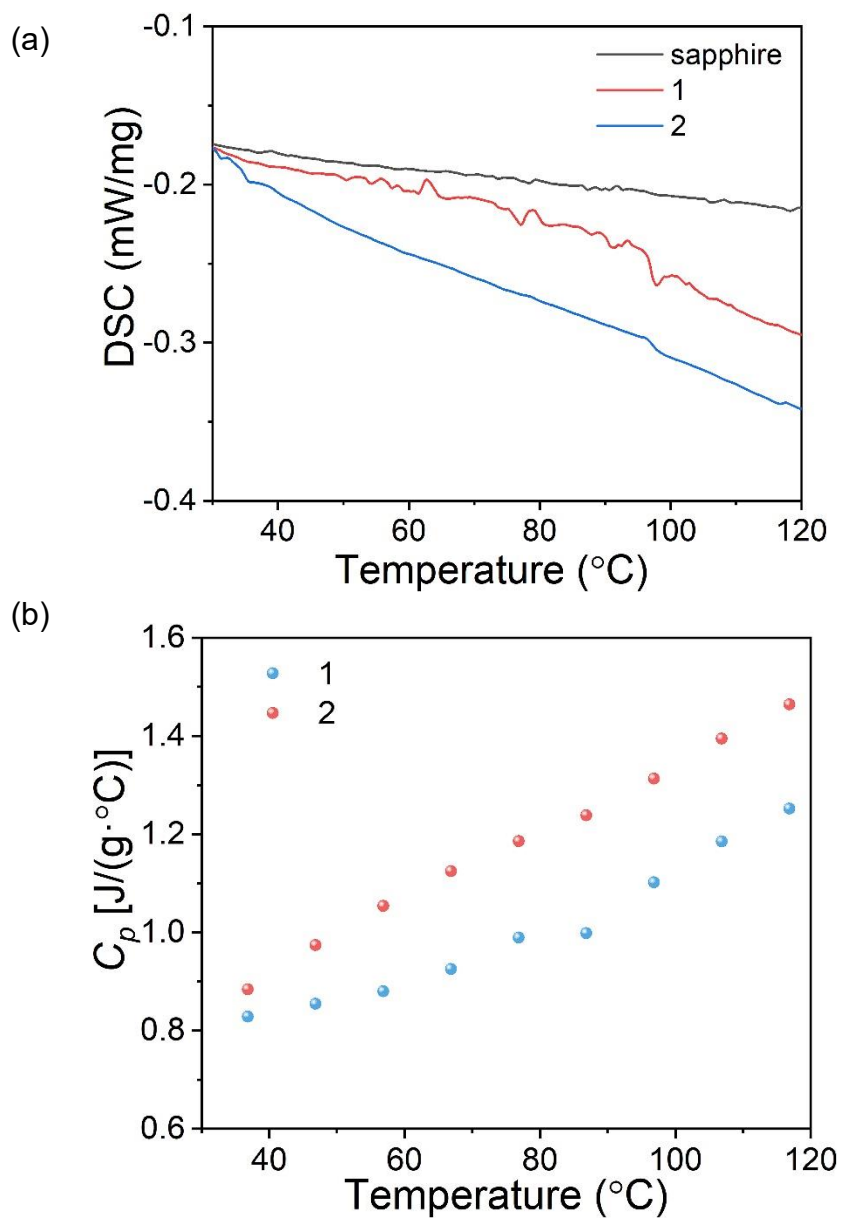


Figure 10. (a) DSC curves, and (b) specific heat capacity of **1** and **2**. The average C_p values of compound **1** and **2** in the temperature range 30 – 100 °C are 0.94 and 1.11 J/g·°C, respectively.

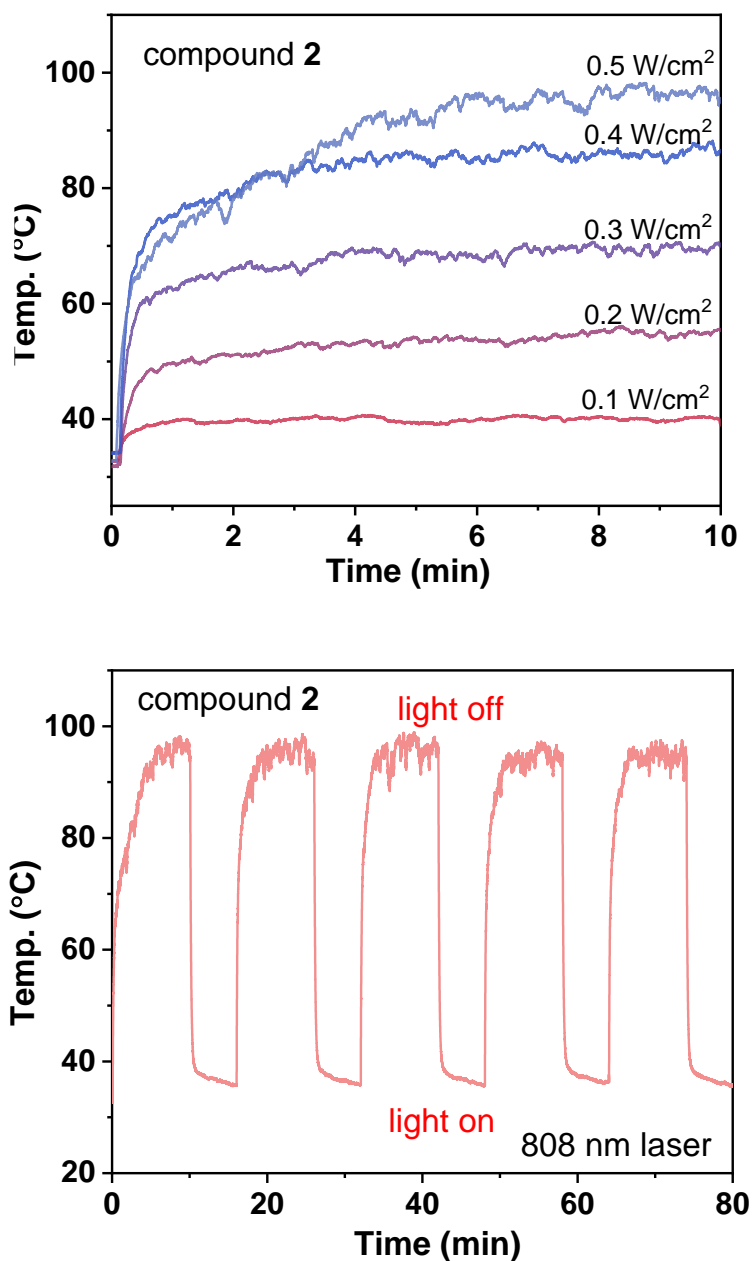


Figure S11. Plots of temperature versus time of **2** under 808 nm laser irradiation with different energy densities and five heating-cooling cycles under 808 nm laser irradiation with a power density of 0.5 W/cm².

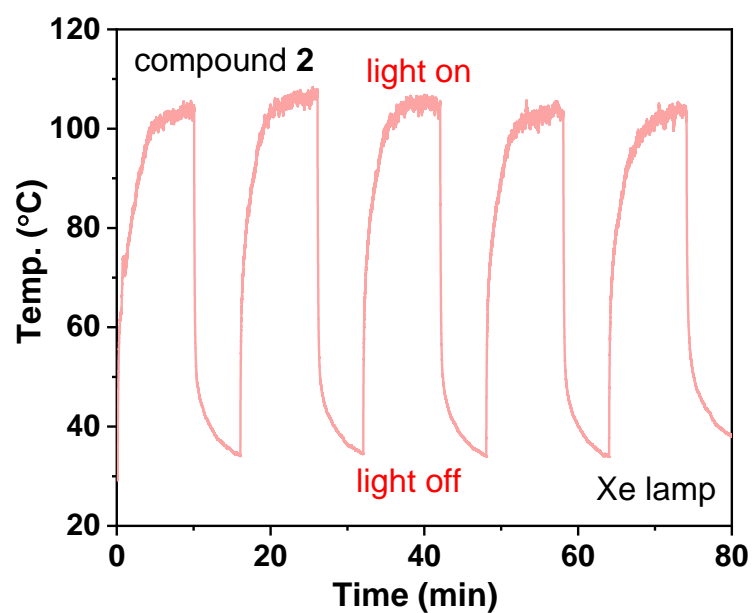
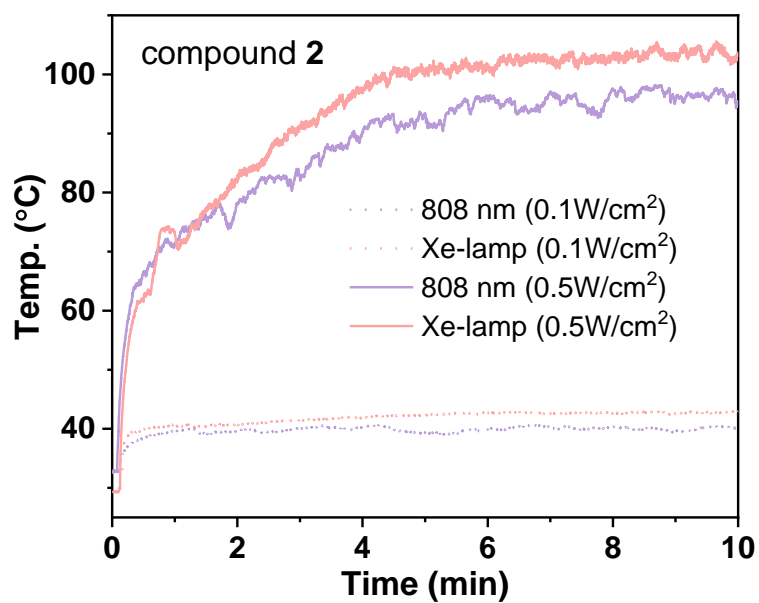


Figure S12. Plots of temperature versus time of **2** under Xe-lamp irradiation with a power density of 0.1 and 0.5 W/cm² and five heating-cooling cycles under Xe-lamp irradiation with a power density of 0.5 W/cm².

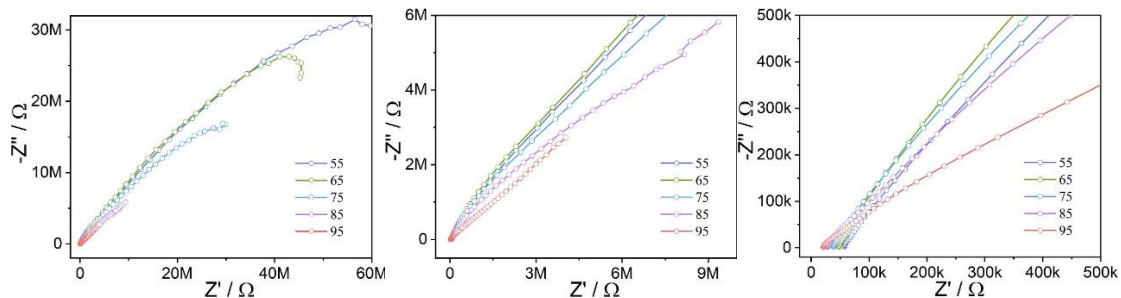


Figure S13. Nyquist plots for the pellet of **1** at 25 °C and various RH. Up: RH increases from 55 to 95%; Middle and Right: The enlarged view of the graph.

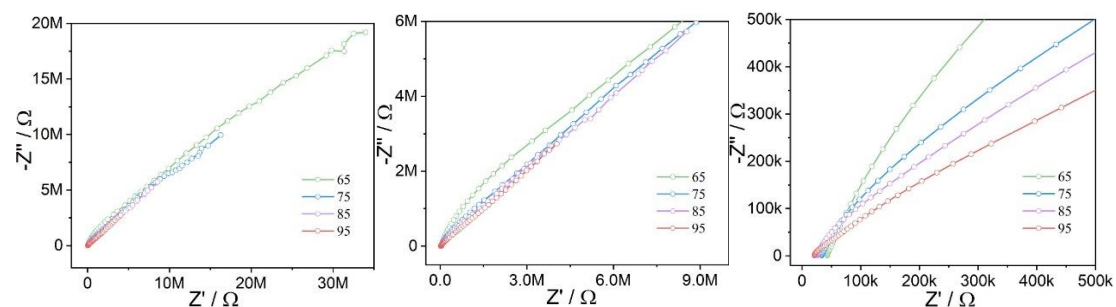


Figure S14. Nyquist plots for the pellet of **1** at 25 °C and various RH. Up: RH decreases from 95 to 65%; Middle and Right: The enlarged view of the graph.

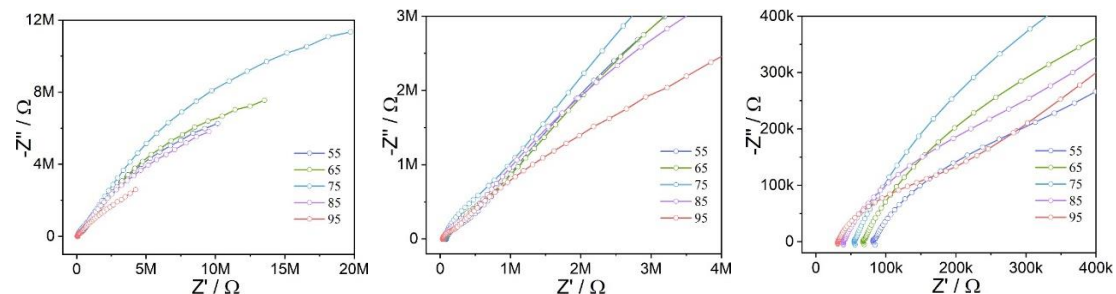


Figure S15. Nyquist plots for the pellet of **2** at 25 °C and various RH. Up: RH increases from 55 to 95%; Middle and Right: The enlarged view of the graph.

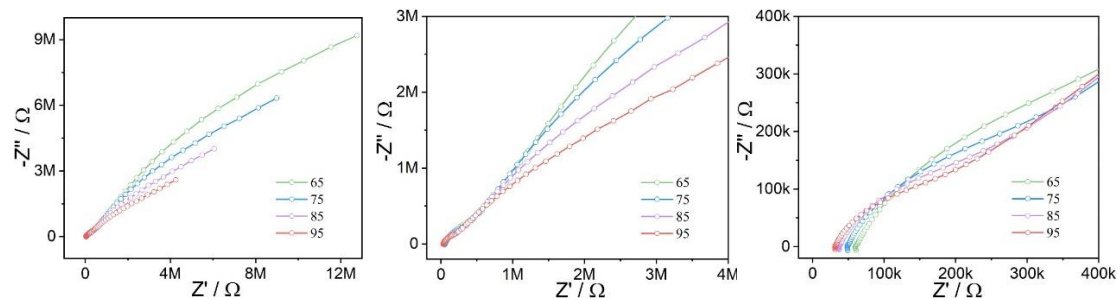


Figure S16. Nyquist plots for the pellet of **2** at 25 °C and various RH. Up: RH decreases from 95 to 65%; Middle and Right: The enlarged view of the graph.

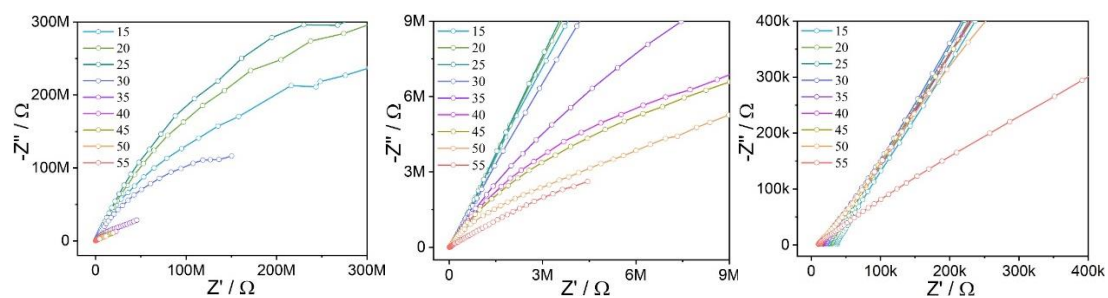


Figure S17. Nyquist plots for the pellet of **1** at 95% RH and various temperatures. Middle and Right: The enlarged view of the graph.

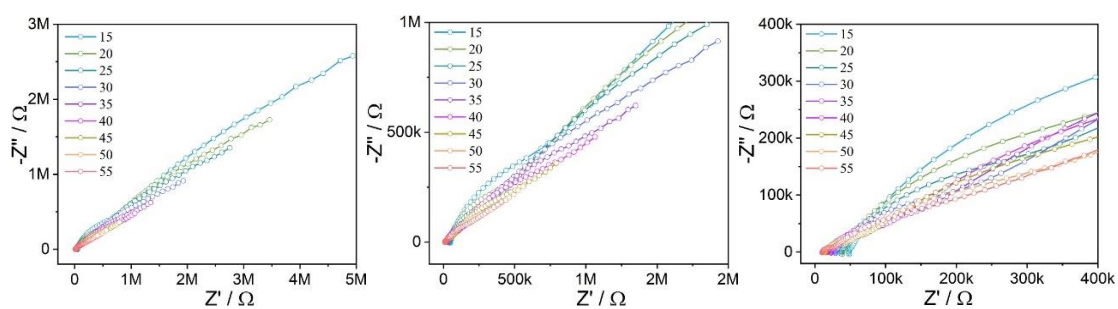


Figure S18. Nyquist plots for the pellet of **2** at 95% RH and various temperatures. Middle and Right: The enlarged view of the graph.

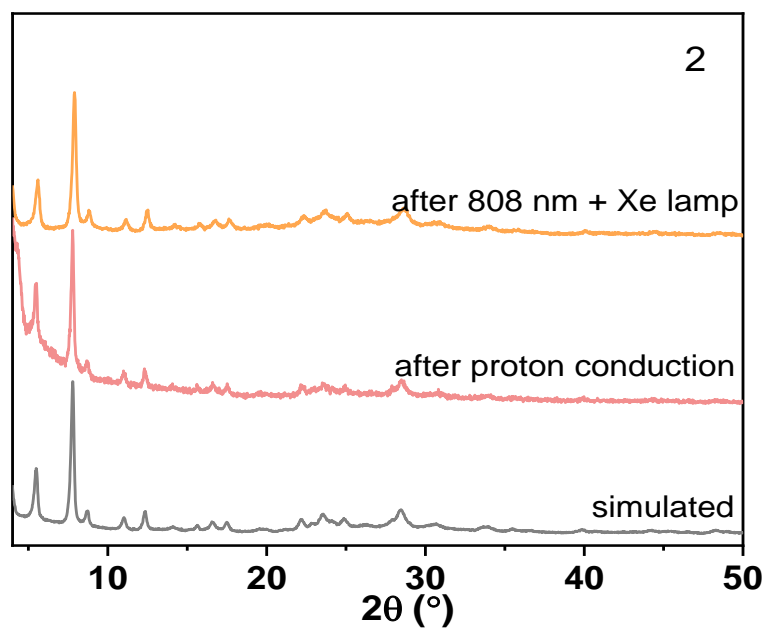
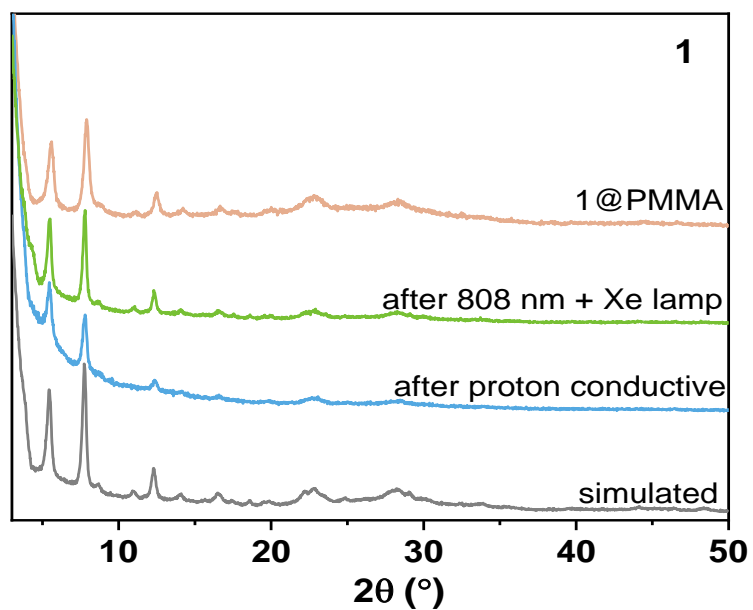


Figure S19. PXRD patterns of **1** and **2** after the proton conductivity and photothermal heating measurements and PMMA-coating procedure. The pattern simulated from the crystal data of **2** is given for comparison.

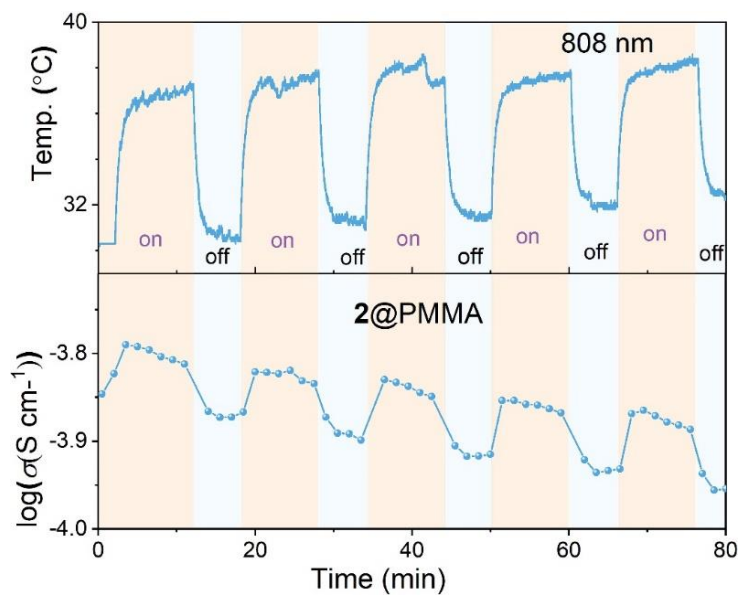


Figure S20. The temperature and proton conductivity variations of **2@PMMA** using the 808 nm laser.